Real-time acquisition of transendothelial electrical resistance in an all-human, *in vitro*, 3-dimensional, blood–brain barrier model exemplifies tight-junction integrity

Zaynah Maherally,*,[1] Helen L. Fillmore,* Sim Ling Tan,[†] Suk Fei Tan,[†] Samah A. Jassam,*
Friederike I. Quack,* Kathryn E. Hatherell,* and Geoffrey J. Pilkington*

*Brain Tumour Research Centre, Institute of Biomedical and Biomolecular Sciences, School of Pharmacy and Biomedical Sciences, University of Portsmouth, Portsmouth, United Kingdom; and [†]Department of Medicine, Faculty of Medicine and Health Sciences, University Putra Malaysia, Serdang, Selangor, Malaysia

ABSTRACT: The blood–brain barrier (BBB) consists of endothelial cells, astrocytes, and pericytes embedded in basal lamina (BL). Most *in vitro* models use nonhuman, monolayer cultures for therapeutic-delivery studies, relying on transendothelial electrical resistance (TEER) measurements without other tight-junction (TJ) formation parameters. We aimed to develop reliable, reproducible, *in vitro* 3-dimensional (3D) models incorporating relevant human, *in vivo* cell types and BL proteins. The 3D BBB models were constructed with human brain endothelial cells, human astrocytes, and human brain pericytes in mono-, co-, and tricultures. TEER was measured in 3D models using a volt/ohmmeter and cellZscope. Influence of BL proteins—laminin, fibronectin, collagen type IV, agrin, and perlecan—on adhesion and TEER was assessed using an electric cell-substrate impedance–sensing system. TJ protein expression was assessed by Western blotting (WB) and immunocytochemistry (ICC). Perlecan (10 μg/ml) evoked unreportedly high, *in vitro* TEER values (1200 Ω) and the strongest adhesion. Coculturing endothelial cells with astrocytes yielded the greatest resistance over time. ICC and WB results correlated with resistance levels, with evidence of prominent occludin expression in cocultures. BL proteins exerted differential effects on TEER, whereas astrocytes in contact yielded higher TEER values and TJ expression.—Maherally, Z., Fillmore, H. L., Tan, S. L., Tan, S. F., Jassam, S. A., Quack, F. I., Hatherell, K. E., Pilkington, G. J. Real-time acquisition of transendothelial electrical resistance in an all-human, *in vitro*, 3-dimensional, blood–brain barrier model exemplifies tight-junction integrity. FASEB J. 32, 168–182 (2018). www.fasebj.org

KEY WORDS: neurovascular unit · extracellular matrix · central nervous system

The blood–brain barrier (BBB) is a dynamic and selective diffusion barrier that is highly restrictive in the transport of substances between the blood and the CNS (1, 2). It also offers a challenge for the passage of bloodborne cells, including white blood cells and circulating cancer cells, entering the brain (3) and is essential for the healthy functioning of the CNS (2).

The BBB is a complex system composed of various cellular components, including brain endothelial cells lining the cerebral vasculature (4), a vascular basal lamina (BL), pericytes embedded within the BL (5), and astrocyte endfeet ensheathing the vessels (1). These components form what is termed the functional neurovascular unit (6).

The tight junction (TJ) network of the BBB is central to its functional integrity and is composed of a strikingly complex pattern of transmembrane protein expression, including junctional adhesion molecules and cytoplasmic proteins associated with TJs (7, 8).

The BL is an additional and vital component of the neurovascular unit because it has specific extracellular

matrix (ECM) molecules that are important for the maintenance of the BBB (9). Indeed, the ECM, which composes the BL and is squeezed between endothelial cells and astrocyte end-feet, has an important role in maintaining the health and function of vascular endothelial cells. The BL is composed of fibronectin, type IV collagen, nidogens, laminin, and heparan sulfate proteoglycans (agrin and perlecan) (10). These ECM proteins are vital for the formation and preservation of the BL (11) and have important roles in cell adhesion, migration, differentiation, and growth (12). Interactions among ECM proteins and other cells influence various signaling pathways, which results in increased expression of the component TJ proteins; therefore, the ECM of the BBB has an essential role in barrier structural integrity and maintenance (13, 14). Collagen IV, laminin, and fibronectin are major constituents of the neurovascular BL (15), with fibronectin having a strong role in cellular adhesion and laminin by being involved in the polarization of cells, an important feature contributing to the BBB properties (15) and constituting the primary ECM component required for BL assembly. Collagen IV is also reported to maintain BL structural integrity (10). Agrin also accumulates extensively in the BL of the brain microvasculature (16). Moreover, a role for agrin in BBB development was highlighted through its accumulation around brain microvessels during chicken and rat embryonic development (17). In parallel, loss of agrin was seen to correlate with a loss of junctional protein expression in the cerebral blood vessels and enhanced BBB leakiness *in vivo* (18, 19), supporting its role in BBB maintenance. Perlecan also appears to have a critical role in basement membrane maintenance and stability (20, 21). Perlecan is most abundant in the CNS capillary BL, interacting with other components of the BL and several growth factors, suggesting it has a role in the formation and stabilization of the BL (20, 22). Deguchi *et al.* (23) suggested that perlecan has an important role in BBB function *via* growth factor regulation, such as fibroblast growth factor, a soluble factor that is likely essential for maintaining BBB integrity.

The cellular components comprising the BBB and the constituents aiding its structure act in concert for it to retain its dynamic functions. Although complex, the need to develop *in vitro* models that include such *in vivo* components/constituents will aid in the discovery of how putative therapeutic agents pass through the BBB, and the underlying mechanisms by which cancer cells from other regions of the body can metastasize to the brain.

There are few reliable, *in vitro* models of the BBB (24); however, although not directly replacing *in vivo* models, *in vitro* models can be improved. The current gold standard method used to measure BBB integrity is transendothelial electrical resistance (TEER) and transendothelial permeability coefficient for small, soluble, inert tracers (25).

Many research groups use nonhuman animals or animal cells to construct BBB models with which to explore cerebral metastasis and delivery of drugs for brain pathologies. Animal models are often considered a more attractive prospect for researchers than human models because access to human components is challenging and higher costs are involved (*e.g.*, human

serum supplementation). However, animal models, both *in vitro* and *in vivo,* contain many apparent protein/antigenic and gene/molecular differences compared with human tissues and models.

To address this concept and circumvent the continued use of nonhuman animal models that may not accurately reflect the human brain and/or the disease under investigation, it is essential to develop and demonstrate the effective utility of reproducible, 3-dimensional (3D), all-human, *in vitro* models that incorporate human cells and ECM components under human serum supplementation conditions. Such models will better simulate the *in vivo* human situation for use in studies of disease pathogenesis and treatment-delivery modalities.

MATERIALS AND METHODS

Cells

Human cerebral microvascular endothelial cell line D3 (hCMEC/D3) cells, immortalized with hTERT catalytic subunits and simian vacuolating virus 40 large T antigens (26), were donated by Dr. Pierre-Olivier Couraud (Institut Cochin, INSERM, Paris, France). Human, healthy, cerebral cortex–derived astrocytes (line SC-1800) and human brain vascular pericytes (HBVPs) were purchased from Caltag Medsystems (Buckingham, United Kingdom). hCMEC/D3 cells were grown in endothelial basal medium 2 (Lonza, Basel Switzerland) supplemented with SingleQuots (Lonza) and 2% human serum (Sigma-Aldrich, St. Louis, MO, USA). SC-1800 were grown in astrocyte basal medium (AGM; Lonza) supplemented with SingleQuots (Lonza) and 3% human serum (Sigma-Aldrich). HBVP were cultured in pericyte basal medium (Caltag Medsystems), supplemented with pericyte growth factors (Caltag Medsystems) and 2% human serum (Sigma-Aldrich). All cells were grown in a 5% CO_2 atmosphere, 37°C incubator. Cell lines were authenticated as human with a microfluidic electrophoresis system incorporating a 2100 Bioanalyzer (Agilent Technologies, Santa Clara, CA, USA) to analyze short tandem repeat PCR fragments from 10 human genomic loci of human cell lines (27). Cells were routinely tested for mycoplasma with a kit from Lonza.

ECM concentrations

The following ECMs were used in the model, based on the manufacturer's recommended working range: recombinant human endorepellin/perlecan (R&D Systems, Minneapolis, MN, USA) at 2.5–10 µg/ml, recombinant human agrin (R&D Systems) at 1–3.5 µg/ml, human collagen type IV (Sigma-Aldrich) at 7–10 µg/ml, laminin from a coculture system of human fibroblasts and epithelial cells that contains the laminin subunit β 1 (Sigma-Aldrich) at 25–75 µg/ml, and fibronectin from human plasma (Sigma-Aldrich) at 1–5 µg/ml.

Antibodies

Primary antibodies

The following antibodies were used: rabbit pAb, IgG, anti–von Willebrand factor (vWF) at 1:100 for immunocytochemistry (ICC); 1:20 for flow cytometry (FC; Abcam, Cambridge, MA, USA), mouse mAb, IgG1, anti–platelet endothelial cell adhesion molecule-1 (PECAM-1, 1:200; 1:20; Abcam), rabbit mAb, IgG, anti-β catenin (1:250; 1:10) (Abcam), rabbit pAb, IgG, anti–α-smooth muscle actin (SMA, 1:100; 1:20; Abcam), rabbit pAb, IgG,

anti–glial fibrillary acidic protein (GFAP; 1:200; 1:25), and mouse mAb, IgG, anti-vimentin (1:500; 1:25; Agilent Technologies) and mouse mAb, IgG, anti-chondroitin sulfate (NG2, 1:500; 1:25; R&D Systems). Rabbit pAb, IgG, anti-occludin (1:200; Abcam) was used for ICC and Western blot (WB). Rabbit pAb, IgG, and anti-cyclophilin A (Abcam) were used as a loading control for WB at 1:10,000.

Secondary antibodies

Fluorochrome-conjugated AlexaFluor-488 and -568 (Thermo Fisher Scientific, Waltham, MA, USA) were used in ICC and FC (1:500). Horseradish peroxidase–conjugated IgG (Thermo Fisher Scientific) was used for chemiluminescent detection in WB (1:1000).

Cytopainter dyes

A CytoPainter cell tracking staining kit (Abcam) was used to uniformly label live cells per the manufacturer's instructions for investigating TJ protein expression in co- and triculture BBB models. Before seeding for subsequent BBB experiments, 1×10^6 endothelial cells were dyed green, astrocytes were dyed red, and pericytes were dyed blue.

Cell proliferation assay

CellTiter 96 Aqueous One Solution cell proliferation assay kit (Promega, Madison, WI, USA) also known as 3-(4,5-dimethyl-thiazol-2-yl)-5-(3-carboxymethoxyphenyl)-2-(4-sulfophenyl)-2H-tetrazolium, inner salt (MTS), was used to assess the proliferation rate of the cells, according to the manufacturer's protocol. Briefly, hCMEC/D3 cells were seeded at 2.5×10^4, 5.0×10^4, 7.5×10^4, and 1.5×10^5 cells/well and incubated at 37°C, 5% CO_2 for 5 d. Subsequently, every 24 h, 20 µl of MTS reagent was added to each well, and cells were incubated further for 3 h at 37°C, 5% CO_2, before being read on a spectrophotometer microplate reader (Polarstar Optima; BMG Labtech, Ortenberg, Germany). Absorbance values were recorded at 490 nm. Each experiment was repeated 3 times in triplicate. A standard curve was previously calibrated at cell densities of 2.5×10^4, 5.0×10^4, 7.5×10^4, 1.0×10^5, and 1.5×10^5 cells/well.

Cell viability assay

Quantitative analysis of viable cells was investigated using the Trypan blue exclusion method, which is based on the principle that the suspension of hCMEC/D3 cells is simply mixed with Trypan blue, then automatically visualized and counted by the Vi-Cell Analyzer using the Vi-Cell XR software (Beckman Coulter, Brea, CA, USA). In that protocol, only nonviable cells take up the dye. Before harvesting cells, the confluency level was visualized with an Olympus (Tokyo, Japan) 1X71 inverted phase-contrast microscope.

ICC

ICC was performed following an established, previously described procedure (28). Briefly, cells were seeded onto sterile coverslips within a 6-well plate at 1×10^5 cells/well, fixed with 4% paraformaldehyde (Sigma-Aldrich) and permeabilized with 0.1% Triton X-100 (Sigma-Aldrich) for intracellular antigen detection, before incubation with the primary antibody. Cells were then incubated with the relevant secondary antibody. Cells were washed with 1× PBS before and after antibody incubation. Nuclei were counterstained with Hoechst Blue (Sigma-Aldrich), and slides viewed using an Axio Imager Z1 fluorescence microscope

(Carl Zeiss, Oberkochen, Germany). Images were captured with Volocity image analysis software (v.5.2; PerkinElmer, Waltham, MA, USA).

FC

FC was performed using standard protocols (28). Cells were seeded in 6-well plates at 2×10^5 cells/well. For intracellular antigen staining, cells were permeabilized with cytofix/cytoperm solution (BD Biosciences, Franklin Lakes, NJ, USA) and blocked in 2% serum/0.2% saporin/PBS (Sigma-Aldrich) before primary antibody incubation, then washed with 0.2% saporin/PBS and incubated with secondary antibodies. After incubation, cells were washed, resuspended in PBS, then transferred to fluorescence-activated cell sorting tubes (BD Biosciences). Propidium iodide (Sigma-Aldrich) was added to samples to ensure viability of cells, except for intracellular antigen detection. Analysis was performed on a 4-color, multiparameter, fluorescence-activated cell sorter (Calibur; BD Biosciences), equipped with a 488-nm argon gas laser and a 635-nm red diode laser. Each sample was analyzed in triplicate plus 1 negative control (primary antibody omitted and isotype control IgG used), and the experiment was repeated 3 times. The expression level was assessed by the percentage of positive cell population.

WB

Cell lysates were separated in the any-kilodalton precast SDS-PAGE gel (Bio-Rad Laboratories, Hercules, CA, USA) and transblotted onto a PVDF membrane (GE Healthcare Life Sciences, Little Chalfont, United Kingdom). Immunodetection was achieved using the primary antibodies and horseradish peroxidase–conjugated secondary antibodies. The blot was then visualized and analyzed with the Gbox Chemi XT16 system (SynOptics Communications, Santa Clara, CA, USA). Cells not coated with any ECM were used as controls.

Confocal microscopy

ICC images were captured using the ×40 oil-immersion objective of a Zeiss meta LSM 510 Axioskop2 confocal microscope. Fluorescence was detected at excitation wavelengths of 488 (green), 568 (red), and 405 nm (blue), with argon, HeNe1, and diode lasers, respectively. Multitrack image capture was used with 2 channels so that separate channels could image different colors to help prevent any overlap in excitation spectra. Identical settings were then used to image negative controls in which the primary antibody was omitted.

Adhesion assays
Quantitative adhesion assay

Plates (96 wells; Greiner Bio-One, Frickenhausen, Germany) were coated with recombinant human endorepellin/perlecan (R&D Systems) at 2.5–10 µg/ml, recombinant human agrin (R&D Systems) at 1–3.5 µg/ml, human collagen type IV (Sigma-Aldrich) at 7–10 µg/ml, laminin from human fibroblasts (Sigma-Aldrich) at 25–75 µg/ml, or fibronectin from human plasma (Sigma-Aldrich) at 1–5 µg/ml and incubated at 37°C, 5% CO_2 for 2 h. Cells at a density of 7.5×10^4 cells/well were seeded onto each of the above substrates. The plate was then incubated for 2 h at 37°C in a CO_2 incubator. Subsequently, unbound cells were vigorously washed away with PBS, and adherent cells were fixed with 4% PBS and stained with crystal violet (0.1% w/v; Sigma-Aldrich). Absorbance of stained nuclei was determined using a plate reader (Polarstar Optima) at 570 nm. All tests were performed in triplicate and repeated 3 times.

Qualitative adhesion assay

hCMEC/D3 cells were labeled with Cytotracker solution for 1 h at 37°C and seeded onto precoated (with optimized differential ECMs) coverslips at a density of 1×10^6/well and grown to confluency. After 3 h incubation at 37°C, cells were washed with PBS, fixed with 4% paraformaldehyde, and stained with Hoechst blue. Coverslips were mounted onto slides with Vectashield and viewed under a fluorescence microscope (Axio Imager Z1). Analysis was performed using the Volocity software.

Resistance monitoring with electric cell substrate impedance sensing

Electric cell substrate-impedance sensing (ECIS) arrays (8W10E+, 8 wells; ibidi, Planegg, Germany) were stabilized with L-cysteine (10 nM, 10 min), washed in HBSS (Thermo Fisher Scientific), and coated with recombinant human endorepellin/perlecan at 2.5–10 µg/ml, recombinant human agrin at 1–3.5 µg/ml, human collagen type IV at 7–10 µg/ml, human fibroblast laminin at 25–75 µg/ml, or human plasma fibronectin at 1–5 µg/ml and incubated at 37°C, 5% CO_2 for 2 h. Cells (7.5×10^4 after seeding-density optimization) were then seeded into each chamber, and cell resistance was monitored at 4000 Hz using an ECIS Zθ (Applied Biophysics, Troy, NY, USA) system for 160 h at 37°C with 5% CO_2. Resistance values were obtained in ohms.

In vitro, human BBB models

Mono-, co-, and triculture BBB models were constructed using hCMEC/D3 cells, SC-1800 astrocytes, and HBVPs. Polycarbonate membrane transwell inserts (24-well tissue cultures, 8-µm porosity; Corning, Corning, NY, USA) were coated with 10 µg/ml human perlecan (R&D Systems) on the apical side and 5 µg/ml human fibronectin (Sigma-Aldrich) on the basal side of the filter. The cell-seeding density for SC-1800 cells and HBVPs was 2.5×10^4/filter and for hCMEC/D3, 7.5×10^4 cells/filter. Depending upon culture combination/setup, SC-1800 cells and HBVPs were seeded on the basal side of the porous filter and left to adhere for 2 h before incubating for 72 h at 37°C, 5% CO_2. hCMEC/D3 cells were then seeded on the apical side of the filter, and TEER measurements were read using both the epithelial volt-ohm meter (EVOM; World Precision Instruments, Sarasota, FL, USA), according to the manufacturer's instructions and the automated cell monitoring CellZscope system (NanoAnalytics, Münster, Germany). EVOM resistance values were measured manually every 5–8 h/d for 160 h, and Ohm's law was applied. The CellZscope system provides noninvasive, continuous monitoring of cell monolayers, measuring contact line capacitance (C_{cl}) as well as resistance, thus rendering a 3D approach to BBB monitoring. In this study, we placed the tissue culture inserts into a 24-well cell module, and the system was incubated (37°C and 5% CO_2); TEER values, expressed in ohm square centimeters, were recorded in real time every hour. High TEER values reflected tight barriers. Electrical C_{cl} was also recorded to validate TEER values. For each experiment, at least 3 replicates were measured. Results are expressed as means ± SEM.

TEER measurements

TEER values obtained in ohm square centimeters using cellZscope cannot be compared directly to measurements using different instruments, such as the ECIS system (Ω) or EVOM (Ω/cm^2) because the parameters, such as the height and the surface area of the inserts, along with the AC frequencies for TEER measurements, differ. With the traditional, chopstick-electrode method, AC current is passed, the voltage is measured, and Ohm's law is applied to calculate the resistance of the monolayer; that system is deemed unreliable because it depends on the position and angle of electrode placement. In the ECIS system, there is no basolateral side because the cells are plated onto the electrode wells, which then need mathematical normalization of the variables mentioned before the TEER can be regarded as a true absolute measure.

Resistance monitoring using xCelligence

An additional system, xCelligence (ACEA Biosciences, San Diego, CA, USA), was used as a comparator to the 3 former systems used routinely in our laboratories. In this study, mono, co-, and triculture BBB models were set up using the Cell Invasion Migration plate 16 and 8-µm porosity membrane (Roche Diagnostics, Indianapolis, IN, USA). The cell-seeding density for SC-1800 cells and HBVPs was 2.5×10^4/filter and 7.5×10^4 cells/filter for hCMEC/D3 cells. Depending on the culture combination/setup, SC-1800 cells and HBVPs were seeded on the basal side of the porous filter membrane and left to adhere for 2 h before incubating for 72 h at 37°C, 5% CO_2. hCMEC/D3 cells were then seeded on the apical side of the filter. The plates were then assembled according the manufacturer's instructions and connected to the xCelligence DP system. Values were expressed as the cell index equating to resistance levels. For each experiment, at least 3 replicates were measured.

Statistical analysis

All experiments were performed 3 times independently in triplicate, unless otherwise stated. All values reported are means ± SEM, unless otherwise stated. Statistical analysis was performed using 1-way ANOVA, followed by Tukey's multiple comparison *post hoc* tests, with a probability of $P < 0.05$ regarded as significant. The software package Prism (v.6.05; GraphPad Software, La Jolla, CA, USA) was used.

RESULTS

To develop the 3D models, we first established the optimal endothelial cell density for obtaining high TEER values, with a goal of being able to reach high resistance values within a reasonable time and for that to be maintained for 20 h to enable testing of compounds crossing the barrier. We therefore conducted several optimization experiments in 2D format using hCMEC/D3 cells.

Characterization of cultured endothelial cells

Established endothelial markers—vWF and PECAM-1 (**Fig. 1**)—were assessed by ICC and FC. Cytoplasmic granular expression of vWF was evenly distributed over the cells, whereas PECAM-1 was widely distributed over the cells but condensed on the leading membrane. FC expression levels of the above-mentioned antigens were 60.92 and 98.98%, respectively (Fig. 1, bottom).

Endothelial seeding densities and TEER

hCMEC/D3 cells were seeded at increasing densities from 2.5×10^4 to 1.5×10^5 cells/cm^2, and resistance was
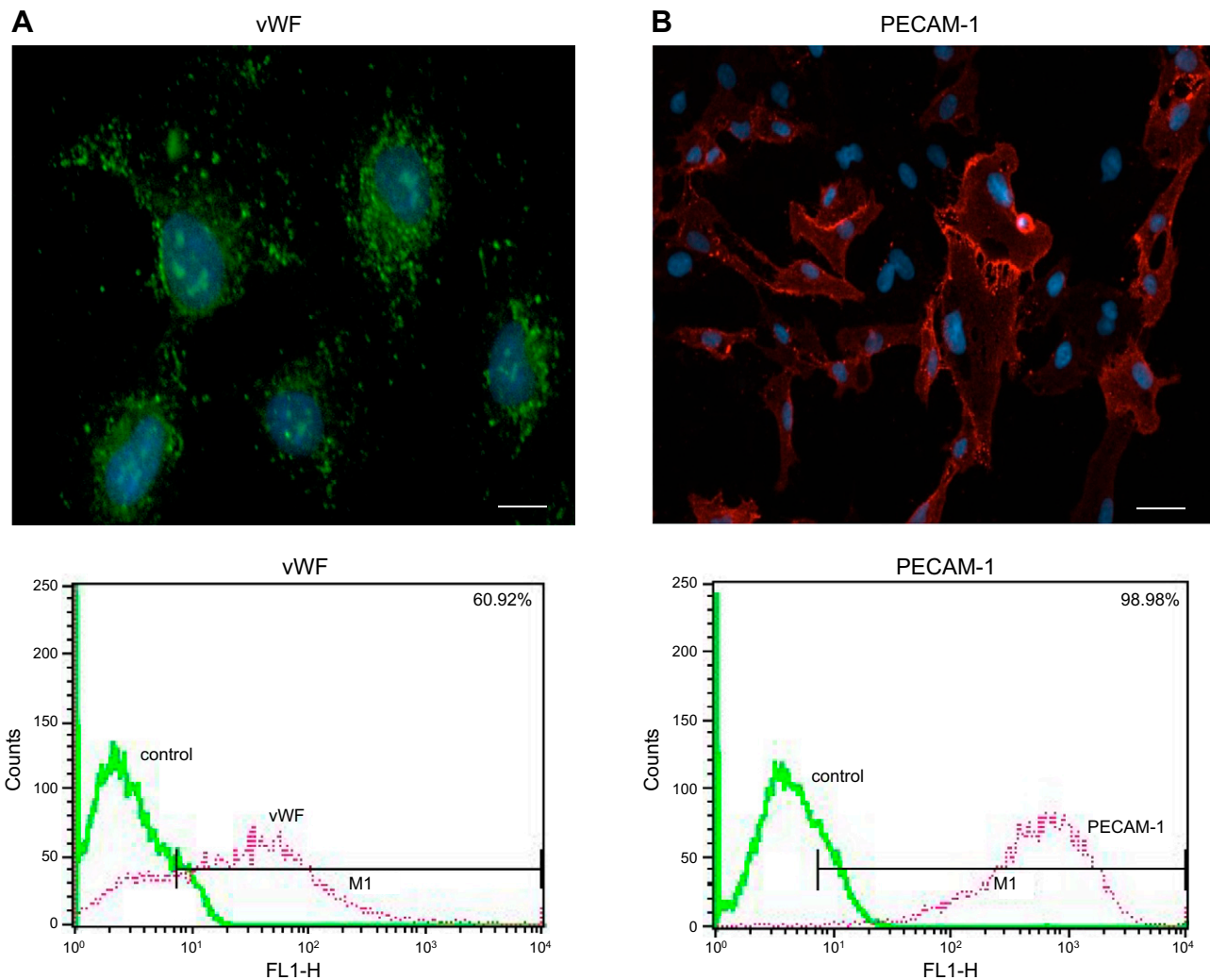
Figure 1. ICC (top) and FC (bottom) showing expression of vWF (*A*) to identify cytoplasmic granules, which were present in endothelium and were expressed at 60.92%, and PECAM-1 (*B*) to identify cellular junction-associated proteins, which were expressed at 98.98% ($n = 3$). Scale bars, 20 μm. For FC, the green graph shows the control (no primary antibody added; isotype controls were used), and the pink graph demonstrates positive expression of previously-mentioned antigens.

recorded for 160 h using ECIS (**Fig. 2***A*). The optimal starting seeding density was determined to be 7.5×10^4 cells/cm^2. At that density, the greatest resistance reached was 920 Ω, achieved at 60 h, where values were maintained above 850 Ω for ~20 h (Fig. 2*A*). Phase-contrast images demonstrated that hCMEC/D3 cells formed monolayers at the 60-h point (Fig. 2*B*) and did not clump. In parallel, the proliferation assay (Supplemental Fig. 1) demonstrated that, at 48–72 h, there was no evidence of proliferation (represented by the constant values/plateau) (red box) supporting the resistance obtained in Fig. 2*A*.

Perlecan and agrin are the most effective BLs in increasing TEER and endothelial adhesion

The next step was to examine the effect of individual BL molecules on hCMEC/D3 cell adhesion and resistance in a 2-D setting to determine optimal ECM concentrations for use in downstream 3D BBB experiments. Five BL molecules, based on the existing literature regarding

CNS BBB, were selected: fibronectin, laminin, collagen IV, agrin, and perlecan. Increasing concentrations of individual ECM components were used to coat wells, followed by the addition of hCMEC/D3 cells (7.5×10^4 cells/cm^2). hCMEC/D3 cell adhesion to individual ECMs was analyzed quantitatively using a crystal violet adhesion assay.

There was an increase in endothelial cell adhesion with increasing concentrations of fibronectin (5 μg/ml), laminin (75 μg/ml), collagen IV (10 μg/ml), and perlecan (10 μg/ml) (**Fig. 3**). Interestingly, the highest concentration of agrin did not correspond to an increase in endothelial cell adhesion; only 1 μg/ml was needed to achieve the highest adhesion (56.2%) ($P < 0.001$) (Fig. 3). In general, adhesion correlated with increased resistance and greater concentrations of individual BL molecules.

Using the optimal BL components, we performed parallel experiments examining resistance, cell adhesion, viability, and motility. The highest TEER values were seen in endothelial cells plated on 10 μg/ml perlecan (1200 Ω),

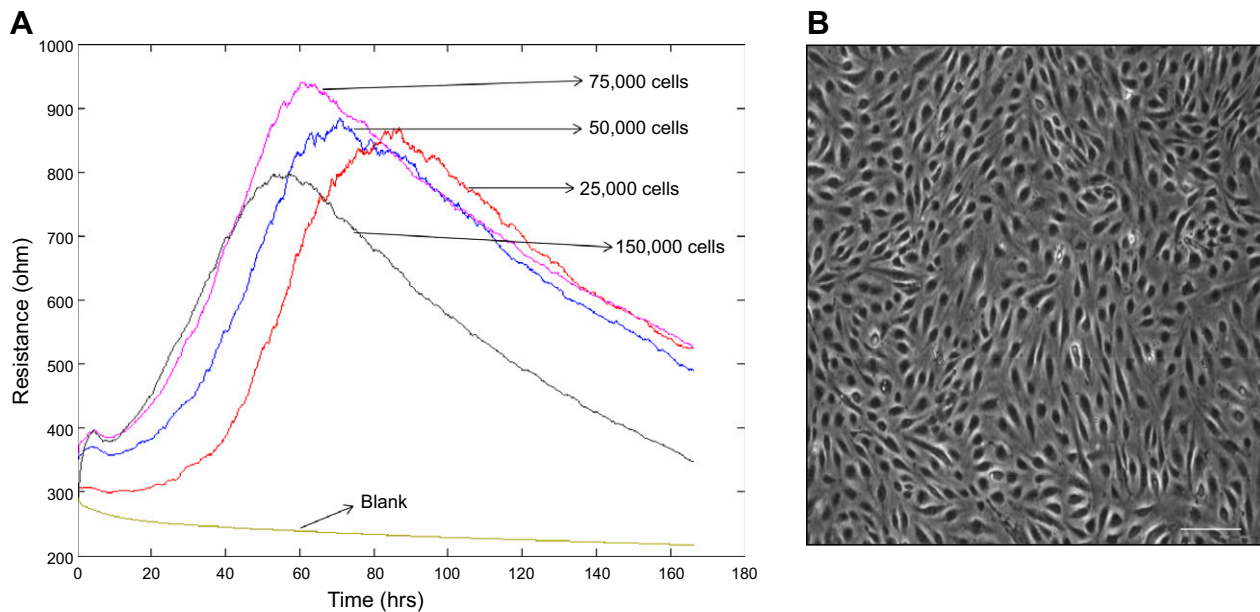**Figure 2.** *A*) Optimal seeding density of hCMEC/D3 cells using ECIS. The optimal seeding density of hCMEC/D3 cells was 7.5×10^4 cells/well, based on the highest TEER value (920 Ω) observed at 60 h. *B*) Morphologic analysis of hCMEC/D3 cells imaged using a phase-contrast microscope at 60 h. Results show a confluent monolayer that correlated with highest TEER values reached in *A*. Scale bar, 20 μm.

followed by 1 μg/ml agrin (980 Ω), 5 μg/ml fibronectin (620 Ω), 10 μg/ml collagen IV (600 Ω), 75 μg/ml laminin (580 Ω), and the control (no BL) at 500 Ω (**Fig. 4***A*) at 60 h ($P < 0.0001$). Under the same conditions, and at the 60-h point, phase-contrast images indicated that endothelial cells seeded on each optimized BL formed a monolayer and contributed to increased resistance (Fig. 4*B*). Those results were in agreement with the quantitative adhesion assay, which demonstrated that the highest adhesion potential was reached when endothelial cells were seeded onto perlecan, followed by agrin, fibronectin, laminin, collagen IV, and the control (no ECM) ($P < 0.01$) (Fig. 4*C*). The viability of cells was assessed using a trypan blue exclusion method over time to determine whether viability of endothelial cells was compromised after BL coating. Results confirmed that there was no effect on the viability of cells (Fig. 4*D*). The motility assay data were in agreement with the adhesion results (Fig. 4*C*). Cells traveled fastest and furthest under no-ECM coating ($n = 30$; $P < 0.05$) (Fig. 4*E*). Highest expression of occludin was observed when endothelial cells were seeded on perlecan and agrin (Supplemental Fig. 2), suggesting an increase in TJ formation, supporting the resistance values obtained in Fig. 4*A*.

Characterization of astrocytes and pericytes

For our next step in 3D model development, we incorporated the use of SC-1800 astrocytes and HBVPs with the hCMEC/D3 cells as described. ICC and FC were conducted using specific known markers to confirm their lineage (**Fig. 5**). SC-1800 cells expressed GFAP and vimentin at 78.50 and 57.90%, respectively. ICC

results demonstrated thread-like staining of GFAP, with an even distribution extending through the cell processes, whereas vimentin showed filamentous dense staining within cell processes (Fig. 5*A*). HBVPs expressed α-SMA and NG2 at 66.50 and 68.30%, respectively. ICC results showed granular expression of α-SMA with a slightly denser expression at process terminals while a relatively even, granular distribution of NG2 was seen (Fig. 5*B*).

Astrocytes and pericytes enhance TEER

The next part of the project was to employ the 3D, "all-human," *in vitro*, BBB model for different functional screening technologies to assess the TEER, including EVOM, the cell automated monitoring system, CellZscope, and xCelligence with different variations of the BBB models (mono-, co-, and triculture combinations). The hCMEC/D3 cells, SC-1800 astrocytes, and HBVPs under human serum supplementation were used in different coculture conditions, and the effect on barrier tightness through resistance readouts were compared when cells were in or out of contact in various culture combinations using the EVOM (**Fig. 6***A*) and only with in-contact simulations using cellZscope (Fig. 6*B*). In those experimental designs, 10 μg/ml of perlecan (previously optimized) was used to precoat wells before seeding. TEER values were obtained over 170 h using the EVOM (**Fig. 7***A*). The optimal TEER value was reached between 80 and 120 h using the endothelial cell in-contact paradigm with astrocytes alone, with TEER values peaking to 450 Ω/cm² at 100 h, followed by out-of-contact cocultures of endotheilal cells + astrocytes (E + A) (385 Ω/cm²)
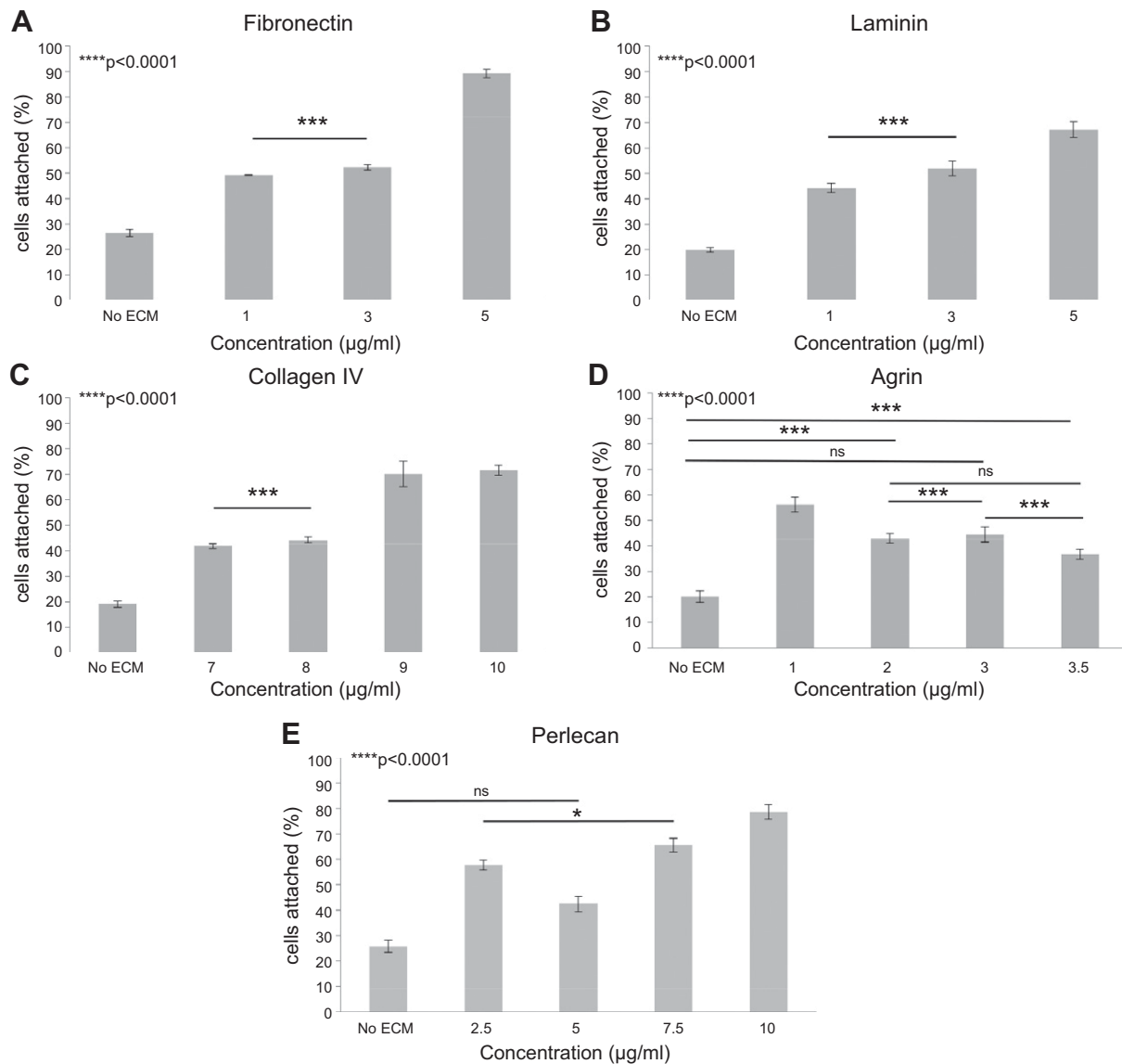
Figure 3. Adhesion of hCMEC/D3 cells at 60 h for fibronectin (*A*) at 1–5 μg/ml, laminin (*B*) at 25–75 μg/ml, collagen type IV (*C*) at 7–10 μg/ml, agrin (*D*) at 1–3.5 μg/ml, and perlecan (*E*) at 2.5–10 μg/ml. Ns, not significant (*n* = 3). *$P < 0.05$, ***$P < 0.001$, ****$P < 0.0001$.

and in-contact triculture of endotheilal cells + astrocytes + pericytes (E + A + P) at 375 Ω/cm^2. Monoculture of endothelial cells alone generated a peak in TEER at 258 Ω/cm^2 at 100 h. The in-contact paradigm resulted in an enhancement of TEER values.

Similar results were obtained when mono-, co-, and triculture models were constructed and their resistance recorded by cellZscope (Fig. 7*B*, top). Results showed greatest resistance was reached when cells were grown in cocultures of E + A (27 $\Omega \cdot cm^2$) at 80 h, followed by tricultures of E + A + P at 22 $\Omega \cdot cm^2$. Monocultures of endothelial cells alone generated a peak at 85 h with resistance at 13.5 $\Omega \cdot cm^2$. Electrical C_{cl} values were also recorded (Fig. 7*B*, bottom), and results showed resistance values increased and C_{cl} decreased, validating the resistance values obtained.

Similar trends were observed *via* the xCelligence system (Supplemental Fig. 3), which produced highest cell

index (equating to resistance values) at 3.0 with cocultures of E + A.

TJ protein expression mirrored TEER

Occludin, β-catenin, and zonula occludens-1 (ZO-1) protein expression, as seen in WB analyses, correlated with resistance measurements. Occludin, β-catenin, and ZO-1 expressions were increased in cocultures of E + A compared to the other culture conditions and when controlled for cyclophilin A (**Fig. 8***A*). Semiquantitative WB analysis demonstrated that, when compared to endothelial cells alone, occludin, β-catenin, and ZO-1 immunoreactivity were greatest with a relative density of 1.6, 1.18, and 1.54 in cocultures of E + A ($P < 0.0001$) followed by tricultures of E + A + P (Fig. 8*B*). ICC results were in agreement with WB analysis, which showed greatest occludin expression (white) in
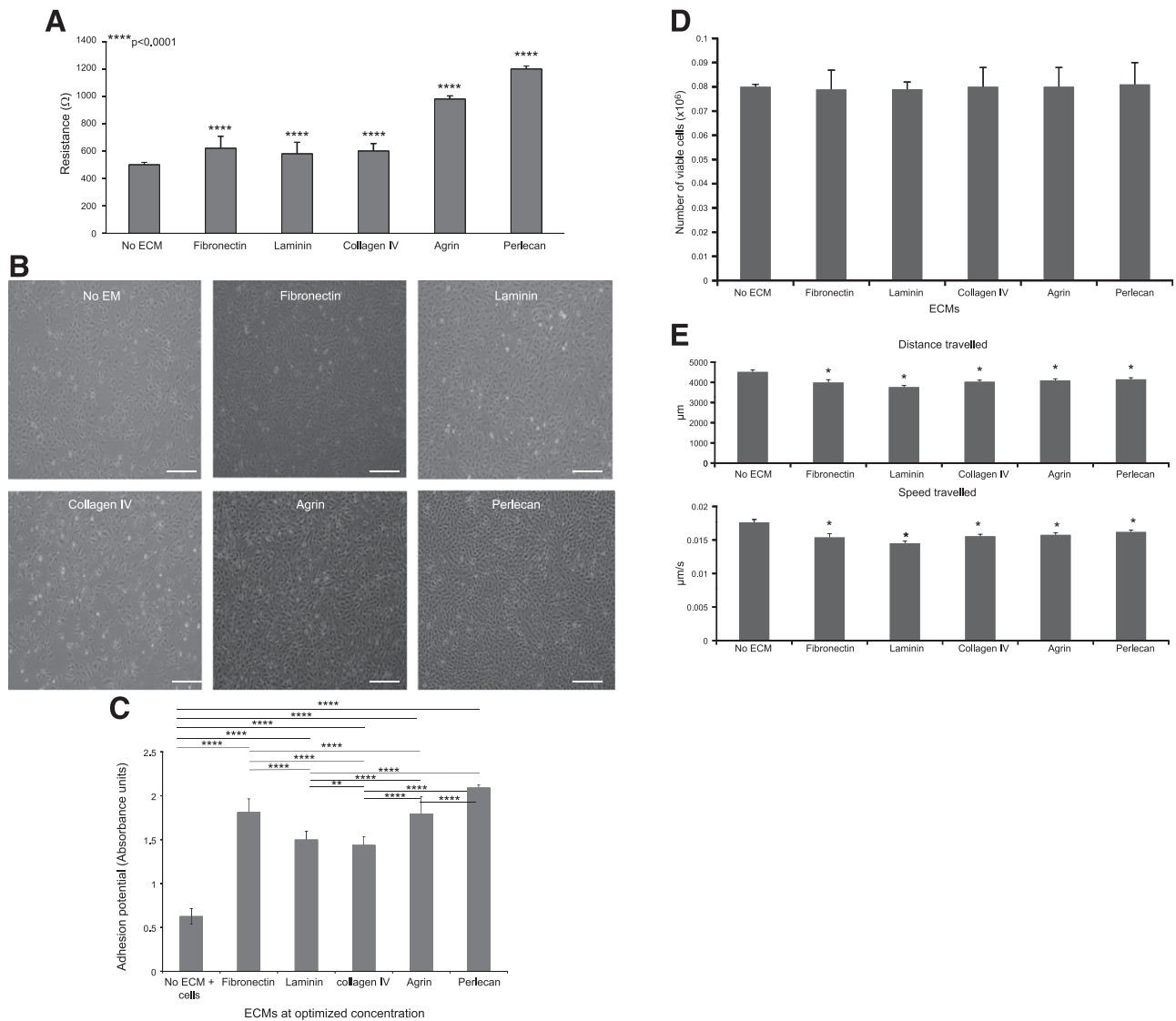
Figure 4. *A*) Resistance with various optimized ECMs. The highest TEER value was reached by coating wells with 10 μg/ml perlecan (1200 Ω), followed by 1 μg/ml agrin (980 Ω), 5 μg/ml fibronectin (620 Ω), 10 μg/ml collagen IV (600 Ω), 75 μg/ml laminin (580 Ω), and the control (no ECM) at 500 Ω. *B*) Phase-contrast images show confluency of hCMEC/D3 cells under brightfield microscopy. Results show that hCMEC/D3 cells adhered best on perlecan. *C*) Quantitative adhesion of hCMEC/D3 cells achieved under various ECMs. Ranking of the highest adhesion potential occurred with endothelial cells seeded onto similar concentrations as in *A*: perlecan, agrin, fibronectin, laminin, collagen IV, and control (no ECM). *D*) Viability of hCMEC/D3 cells under different ECMs. Results show the viability of cells was not affected when treated with different ECMs. *E*) Motility of hCMEC/D3 cells under different ECMs. Cells traveled fastest and furthest under no ECM [$n = 3$ (*A*, *C*); $n = 30$ (*E*)]. *$P < 0.05$, **$P < 0.01$, ****$P < 0.0001$. Scale bars, 20 μm.

cocultures of E + A compared with mono- and tricultures (Fig. 8*C*).

BBB integrity was maintained in model systems

Additional experiments were conducted to confirm BBB integrity. Evans blue was added to various culture configurations, and resistance was measured using EVOM. After coculture of E + A, simulation reached a maximum resistance at 410 Ω/cm² at 90 h. Resistance was recorded with EVOM after the addition of Evans blue for 24 h. Results showed that Evans blue did not cause any significant effect on the resistance values,

suggesting barrier integrity was maintained ($P < 0.001$) (**Fig. 9**).

DISCUSSION

The major goal of this study was to develop a reproducible and reliable, *in vitro*, BBB model that included cell types and components to better reflect the *in vivo* situation when compared with existing published models. We also aimed to ensure that this model maintained a reproducible, intact barrier to adequately test the ability of therapeutics to cross the BBB. It was thus felt to be essential to use human cells and human serum.
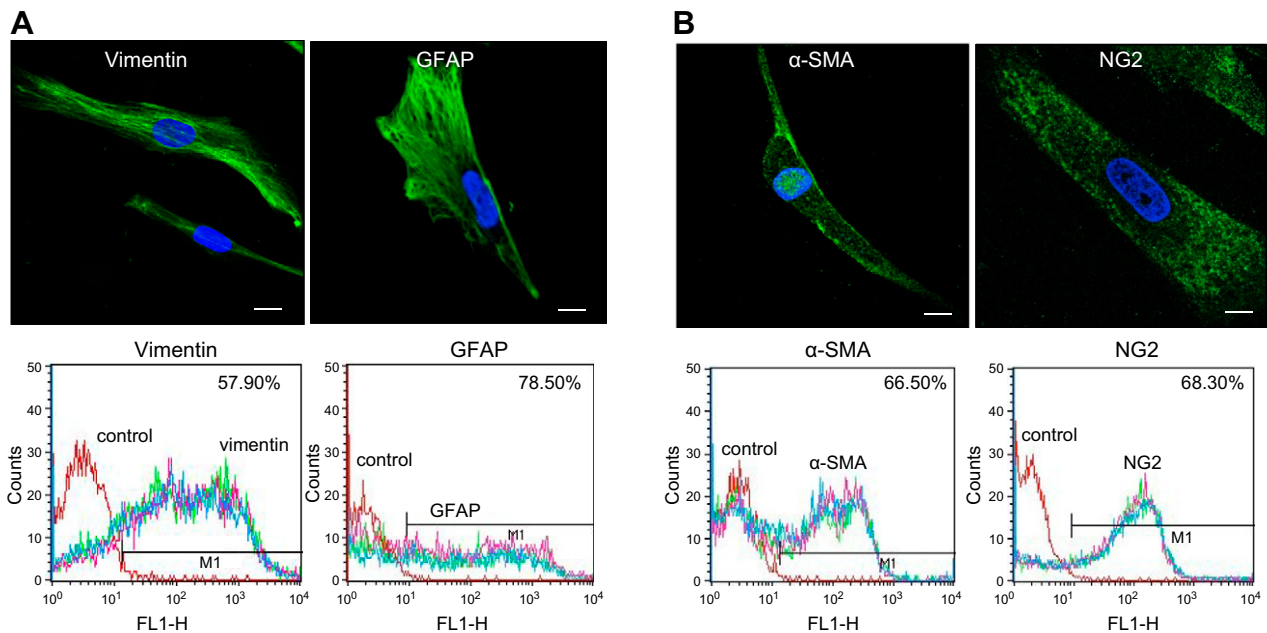
Figure 5. Cells used to construct the BBB model assessed by ICC (top) and FC (bottom). *A*) Astrocyte markers GFAP (right) and vimentin (left). Thread-like staining of GFAP with an even distribution extending through the cell processes. Vimentin showed filamentous staining, denser toward the cell processes. Flow results show expression of GFAP and vimentin to be 78.50 and 57.90%, respectively. *B*) Pericyte markers α-SMA (left) and NG2 (right). ICC results show granular expression of α-SMA with a slightly denser expression around the base of the process. A relatively even granular distribution of NG2 was seen. Flow results show expression of α-SMA and NG2 to be 66.50 and 68.30%, respectively ($n = 3$). Scale bars, 20 μm. For FC, the red graph shows the control (no primary antibody was added; isotype controls were used); the blue, pink, and green graphs demonstrate positive expression of above-mentioned antigens.

We confirmed the cells used were of human origin (by DNA fingerprinting) and that they were indeed endothelial cells, astrocytes, and pericytes (as analyzed by both ICC and FC). Positive ICC expression was gained for all target proteins investigated; vWF and PECAM-1 for hCMEC/D3 cells, GFAP and vimentin for SC-1800 astrocytes, and α-SMA and NG2 for HBVPs.

vWF and PECAM-1 (CD31) were selected as markers because of their specific expression in brain endothelial cells (26, 29, 30), and GFAP and vimentin were selected as astrocyte markers (31–33). There is, at present, no antigenic marker available for all pericytes within the body because of their diverse characteristics and range of functions in a variety of organs (34). However, because of their contractile nature, the presence of α-SMA is frequently evidenced on human vascular pericytes. NG2 has also been shown to be expressed on pericyte cell surfaces during angiogenesis and other vascular processes (34). Indeed, expression of both α-SMA and NG2 has been found to be unique characteristics of pericytes located in neural tissue; thus, their positive expression confirmed the authenticity of HBVPs (35).

Little has been reported on BL components and their influence on human brain endothelial cell and BBB integrity *in vitro*. In particular, information gained in the present study concerning agrin and perlecan and their influence on human brain endothelial cells in this context is novel. Our data showing the influence of agrin and perlecan on BBB integrity do, in fact, correlate with previously published reports *in situ/in vivo* (18, 20). It was reported that the heparan sulfate proteoglycan agrin, which is expressed in the astroglial basement membrane (36, 37), stabilizes the junctional localization of the TJ proteins VE-cadherin, β-catenin, and ZO-1 in mouse brain endothelial cells *in vitro* (38). Further reports show that agrin expression correlated with BBB development and maintenance (39). In parallel, loss of agrin, followed by loss of TJ molecules in endothelial cells of human patients with glioma indicated a direct correlation between the presence of agrin and BBB integrity (18). Agrin is also known as a major binding protein for α-dystroglycan, which suggests an involvement in anchoring endothelial cells and astrocytes to the BL (40).

Perlecan, another heparan sulfate expressed by astrocytes [Winkler *et al.* (41)], has an important role in BL maintenance and stability (11). Perlecan also serves as a signaling platform within the BBB by providing proper cell–cell interaction, which occurs *via* binding to, and signal through, integrin and dystroglycan receptors located on both endothelial cells and astrocytes (42). Previous studies also showed that a lack of perlecan *in vivo* led to disrupted BL and even death in transgenic mice (20, 43, 44). Thus, we have provided an accurate human *in vitro* system, which mirrors mouse-based *in vivo* findings. In our model, perlecan and agrin, as opposed to other commonly used ECM molecules, were superior in obtaining high TEER values as well as high endothelial cell adherence, which suggests that both perlecan and agrin expression may be under the control of endothelial/astrocyte interactions.
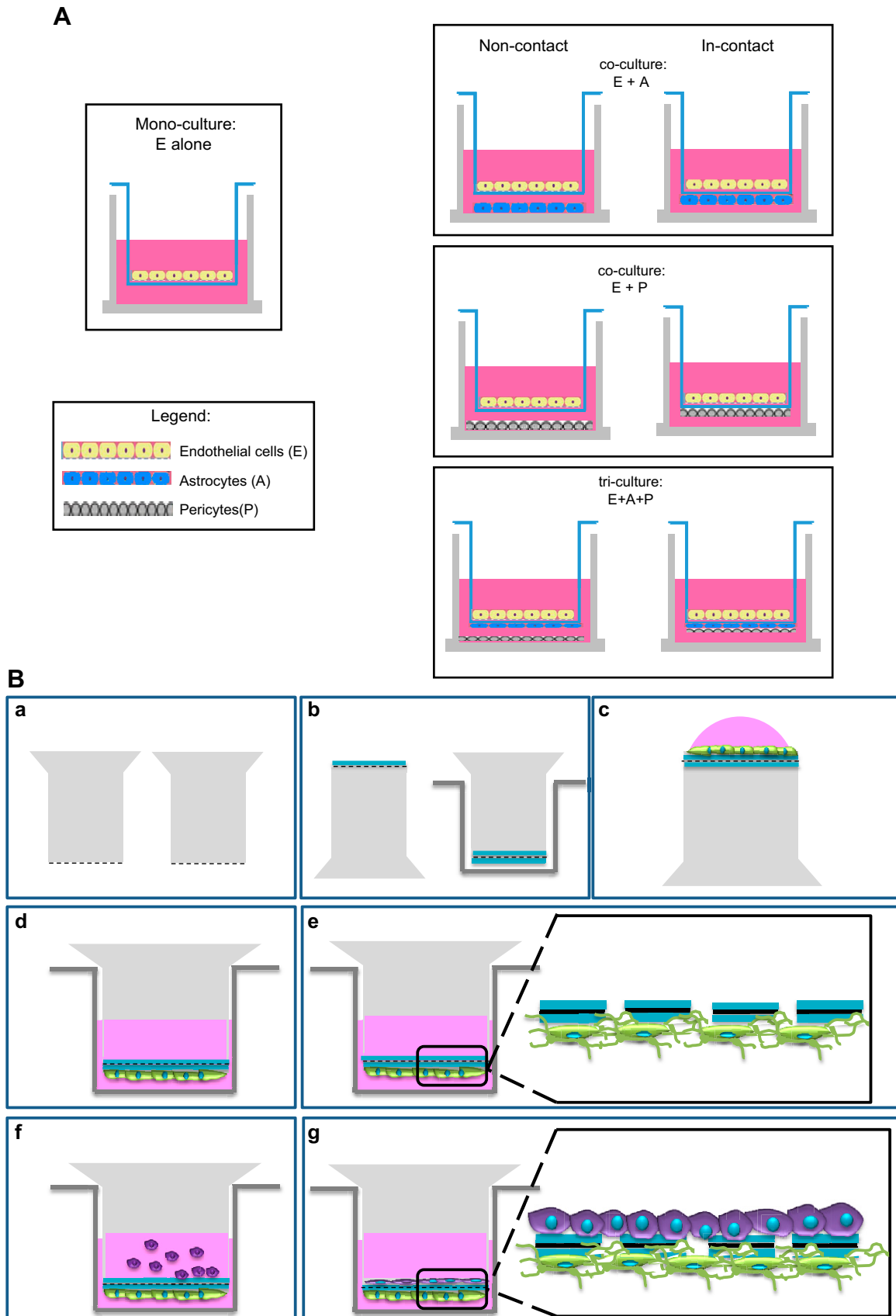
Figure 6. *A*) *In vitro*, all-human, BBB model based on mono-, co-, tricultivation transwell layout for in- and out-of-contact simulations. hCMEC/D3 cells grown as a monoculture, hCMEC/D3 and SC-1800 cells or hCMEC/D3 cells and HBVPs as a coculutre, and hCMEC/D3 cells, SC-1800 cells, and HBVPs as a triculture. *B*) Schematic assembly of BBB model. *a*) Twenty-four-well format, 8-μm
(*continued on next page*)

Figure 7. *A*) Mono-, co-, and triculture models constructed using 8-μm pore size polycarbonate-membrane filters within 24-transwell inserts, using both in- and out-of-contact cell combinations, and their resistance was evaluated by measuring TEER values with EVOM. Results show the highest resistance was reached when cells were grown in coculture and in contact (E + A, endothelial cells + astrocytes; 450 Ω/cm^2) at 100 h, followed by out-of-contact coculture (E + A) at 385 Ω/cm^2 and in-contact triculture (E + A + P, endothelial cells + astrocytes + pericytes) at 375 Ω/cm^2. *B*) Mono-, co-, and triculture models were constructed using 8-μm pore size, polycarbonate, 24-well plate, transwell inserts precoated with 10 μg/ml of perlecan, and their resistance was evaluated by measuring TEER values (top) and C_{cl} (bottom) using cellZscope. Results show highest resistance was reached when cells were grown in coculture (EA, endothelial cells + astrocytes; 27 $\Omega \cdot cm^2$) at 80 h, followed by triculture (EAP, endothelial cells + astrocytes + pericytes) at 22 $\Omega \cdot cm^2$ (top). Results show that as the resistance increases, the C_{cl} decreases, validating cell attachment and spreading (bottom). EP, endothelial cells + pericytes; E, endothelial cells only; AP, astroctes + pericytes.
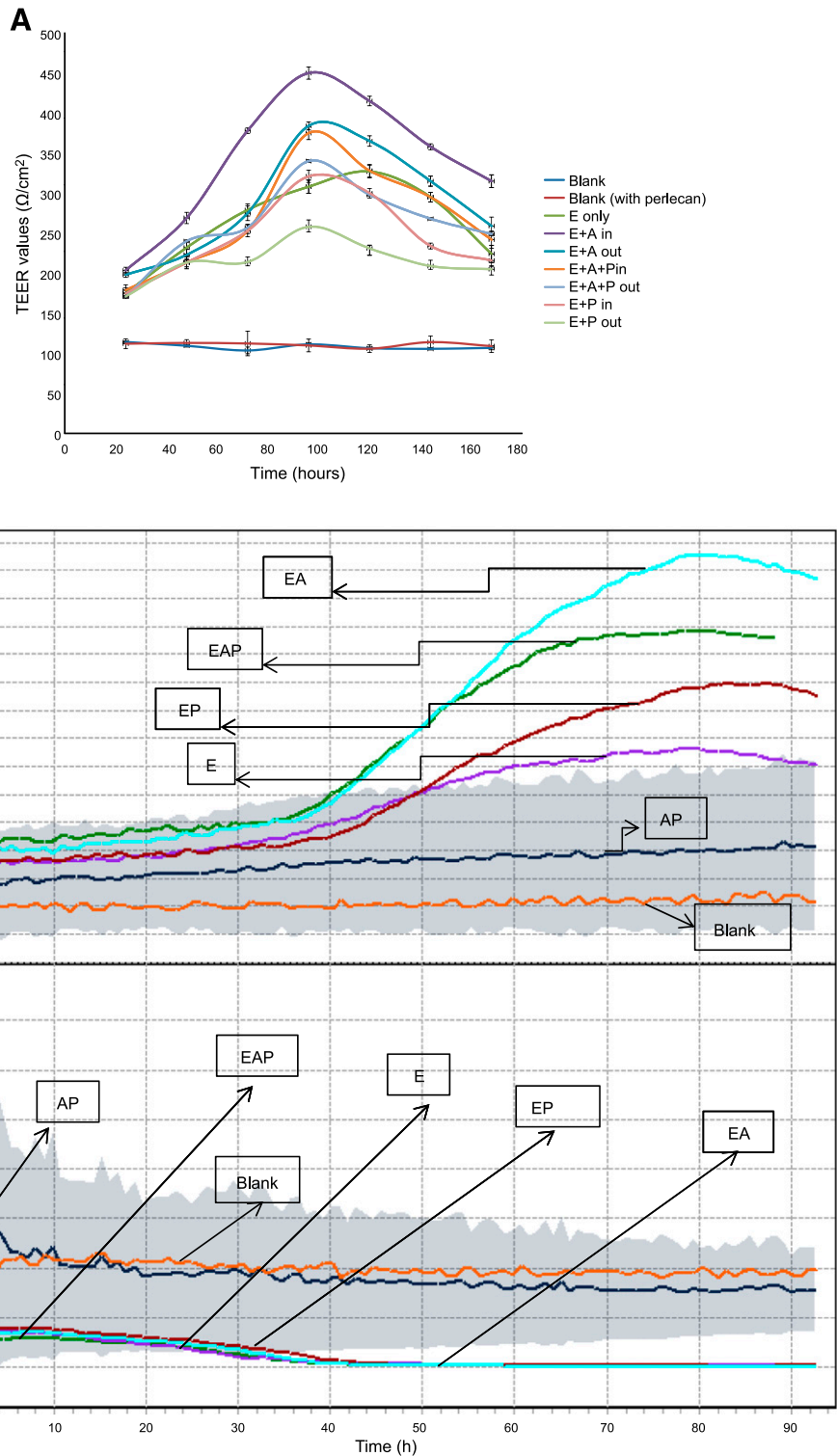
Upon validating our 3D BBB model, we observed that coculturing endothelial cells and astrocytes and in-contact simulation produced the highest resistance compared with other culture configurations. These findings were consistent in all 4 technologies used within the scope of the study, namely, EVOM, ECIS, cellZscope, and xCelligence.

pore size, polycarbonate membrane transwell inserts used. *b*) Both sides of the filters were coated with 10 μg/ml perlecan and left to absorb the EMC for 1 h in the hood. *c*) Depending on culture combinations, astrocytes or pericytes or both were seeded at 2.5×10^4 cells/insert on the lower side of the filters with a positive meniscus and left to adhere for 1–2 h in the hood. *d, e*) Inserts were inverted and placed in the plate containing 600 μl medium and left to incubate for 72 h at 37°C. *f*) hCMEC/D3 cells at 2.5×10^4 cells/insert were then seeded on the top side of the filter. *g*) The combination setup was then placed in the incubator and connected to a CellZscope instrument to read resistance values.
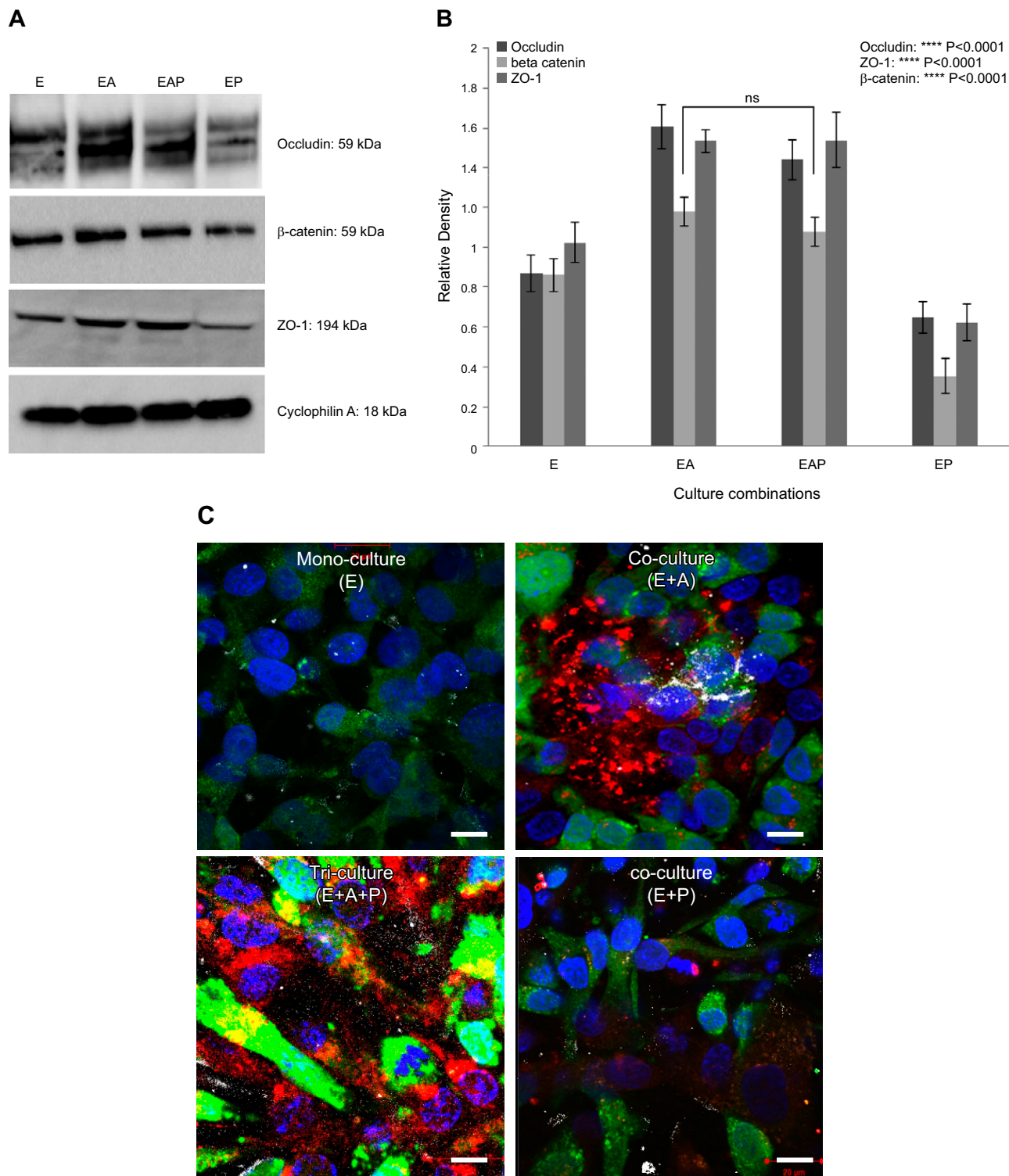
Figure 8. Expression of the TJ proteins occludin, β-catenin, and ZO-1, depicting tightest junction formation when endothelial cells were cocultured with astrocytes. *A*) WB of proteins from BBB culture combinations seeded onto 10 µg/ml perlecan. E, endothelial cells alone; EA, endotheilal cells + astrocytes; EAP, endothelial cells + astrocytes + pericytes; EP, endothelial cells + pericytes. *B*) Semiquantitative analysis using densitometry from *A* showed the highest occludin, β-catenin, and ZO-1 expression (59, 87, and 194 kDa) was seen in coculture (EA), followed by triculture (EAP), monoculture (E), and coculture (EP). Cyclophilin A was used as a protein-loading control ($n = 3$). ****$P < 0.0001$. *C*) ICC images show prominent occludin expression (white) when cells were cocultured (E + A) compared with the other culture setups. The results confirmed our findings in Fig. 7*A, B*. Cells were stained with cytopaint dyes as follows: endothelial cells (green), astrocytes (red), and pericytes (blue). Scale bars, 20 µm.

These findings are supported by both human (45) and animal (25, 46–48) studies where co- and tricultivation of astrocytes and/or pericytes with endothelial cells, significantly increases the tightness of endothelial monolayers. In our previously published studies, we confirmed the coculture model permutation of endothelial cells and
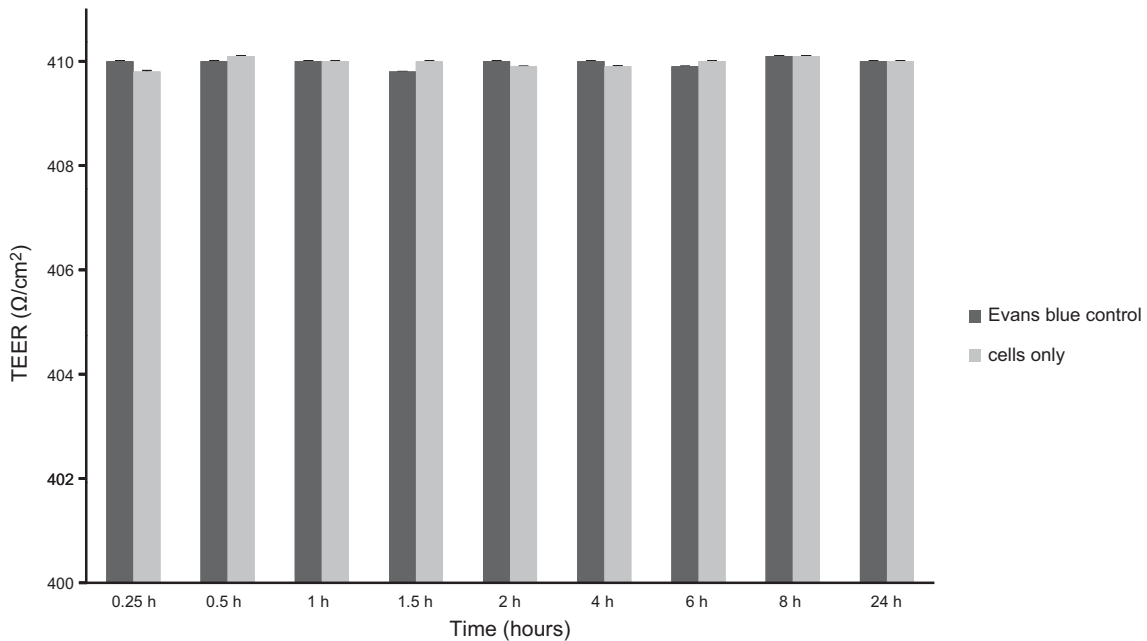
Figure 9. Effect of Evans blue on a coculture BBB model to test for barrier integrity. Resistance was evaluated using EVOM. No change in resistance values was recorded after the addition of Evans blue on a coculture BBB model, suggesting Evans blue did not cross the barrier. $P < 0.001$.

astrocytes was most effective in enhancing barrier properties (45). In this article, we showed that coculturing endothelial cells with astrocytes in contact produced the highest TEER value, suggesting that endothelial cells respond positively to the soluble factors produced by astrocytes, which corresponds to the *in vivo* situation. This finding concurs with those of previous studies which highlighted that direct contact of endothelial cells with astrocytes in cocultures induced expression of BBB specific phenotypes in cocultivation such as increased mitochondrial number and increased TEER (4, 49). Kacem *et al.* (50) also reported through previous anatomic examination of brain microvasculature, that end-feet of astrocytes form a lacework of fine lamellae to closely support the outer surfaces of the endothelium. Studies that investigated coculturing bovine endothelial cells and astrocytes on the upper and lower surfaces of a membrane showed reduced permeability and increased TJ-like structures characteristic of the BBB *in vivo* (51). Further reports have also highlighted the positive influence of glia on induction of BBB properties when endothelial cells and astrocytes were cultured in contact (4). Moreover, Garcia *et al.* (52) showed that coculturing endothelial cells with astrocytes in a cell–cell contact schema increased TJ proteins, such as occludin, and up-regulated P-glycoprotein on endothelial cells. More recently, Yamamizu *et al.* (53) demonstrated enhanced TEER values when coculturing human-induced pluripotent stem cells differentiated into culturally induced brain endothelial cells with astrocytes compared with endothelial cells alone.

For the addition of a third cell type in our model, unlike other previous studies, in which incorporation of pericytes in BBB cultures yielded higher TEER values (46), ours did not. In fact, adding pericytes to our cultures led to a decrease in resistance in our human models. Our BBB simulation of triculturing endothelial cells, astrocytes, and pericytes produced a lower TEER value compared with the coculture arrangement of endothelial cells and astrocytes alone. There may be several explanations why pericytes had a negative effect on the formation of TJs in this model. Similar results have been obtained in previous studies, which suggest that pericytes may act as a barrier, stopping soluble astrocyte factors from reaching endothelial cells (45). The presence of pericytes may trigger matrix metalloprotease (MMP) production through TNF-α, TGF-β, and IL-6. As MMPs have been shown to contribute to BBB regulation *via* the ECM, increased or overexpression of MMPs may result in BBB disruption (54). Alternatively, pericytes, which are highly motile cells and are frequently seen on nonperivascular locations within the brain, may, in our 3D *in vitro* systems display anchorage differences from those in *in vivo* microenvironments; indeed, this is a focus of our ongoing research programs.

Interestingly, in agreement with previous studies that reported an endothelial–pericyte coculture increase in TEER values (1, 35), we showed that coculture of endothelial cells and pericytes yielded higher TEER values compared with an endothelial monolayer alone. This finding confirms the importance of pericytes in forming and maintaining the integrity of TJs (55, 56). Findings showed that the use of CNS pericytes or pericyte-conditioned medium regulated the localization of claudin-5 and occludin in cultured endothelial cells, strengthen barrier integrity and increasing the TEER of endothelial cells *in vitro* (56, 57, 58). Other studies have also highlighted abnormal expression of TJs in endothelial cells in pericyte-deficient mice (56, 59).

In the present study, the most effective culture simulation for increasing TEER values and TJ protein expression was the in-contact coculture model of endothelial cells

with astrocytes. Our findings confirm the cellular communication and importance of astrocytes in inducing barrier function and maintaining barrier integrity. We also showed that coculturing endothelial cells with pericytes yielded higher TEER values compared with a monolayer of endothelial cells, thus confirming the crosstalk of pericytes in contributing to barrier tightness.

Moreover, this study is novel with respect to the addition of human-derived ECMs, human supplementation, and the sole use of human brain–derived cells in various combinations and in both contact and noncontact configurations. The unprecedentedly high TEER levels ($>1000\,\Omega$) achieved *in vitro* also endorse the use of such human model systems. We believe this increases knowledge on BBB biology and closely mimics the *in vivo* situation, providing an effective method for high-throughput screening of preclinical nanoparticle-mediated therapeutic delivery to the brain and investigating the transendothelial migration mechanism of cancer cells in brain metastasis. [FJ]

AUTHOR CONTRIBUTIONS

Z. Maherally, H. L. Fillmore, and G. J. Pilkington designed the research and wrote the paper; Z. Maherally, S. L. Tan, S. F. Tan, S. A. Jassam, F. I. Quack, and K. E. Hatherell performed the research; and Z. Maherally and H. Fillmore analyzed the data.

REFERENCES

1. Dohgu, S., Takata, F., Yamauchi, A., Nakagawa, S., Egawa, T., Naito, M., Tsuruo, T., Sawada, Y., Niwa, M., and Kataoka, Y. (2005) Brain pericytes contribute to the induction and up-regulation of blood–brain barrier functions through transforming growth factor-β production. *Brain Res.* **1038**, 208–215
2. Ballabh, P., Braun, A., and Nedergaard, M. (2004) The blood-brain barrier: an overview: structure, regulation, and clinical implications. *Neurobiol. Dis.* **16**, 1–13
3. Wilhelm, I., Molnár, J., Fazakas, C., Haskó, J., and Krizbai, I. A. (2013) Role of the blood–brain barrier in the formation of brain metastases. *Int. J. Mol. Sci.* **14**, 1383–1411
4. Abbott, N. J. (2002) Astrocyte-endothelial interactions and blood–brain barrier permeability. *J. Anat.* **200**, 629–638
5. Sims, D. E. (2000) Diversity within pericytes. *Clin. Exp. Pharmacol. Physiol.* **27**, 842–846
6. Abbott, N. J., Rönnbäck, L., and Hansson, E. (2006) Astrocyte-endothelial interactions at the blood–brain barrier. *Nat. Rev. Neurosci.* **7**, 41–53
7. Wolburg, H., and Lippoldt, A. (2002) Tight junctions of the blood–brain barrier: development, composition and regulation. *Vascul. Pharmacol.* **38**, 323–337
8. Sandoval, K. E., and Witt, K. A. (2008) Blood–brain barrier tight junction permeability and ischemic stroke. *Neurobiol. Dis.* **32**, 200–219
9. Muramatsu, R., and Yamashita, T. (2014) Pericyte function in the physiological central nervous system. *Neurosci. Res.* **81–82**, 38–41
10. Díaz-Flores, L., Gutiérrez, R., Madrid, J. F., Varela, H., Valladares, F., Acosta, E., Martín-Vasallo, P., and Díaz-Flores, L., Jr. (2009) Pericytes: morphofunction, interactions and pathology in a quiescent and activated mesenchymal cell niche. *Histol. Histopathol.* **24**, 909–969
11. Baeten, K. M., and Akassoglou, K. (2011) Extracellular matrix and matrix receptors in blood–brain barrier formation and stroke. *Dev. Neurobiol.* **71**, 1018–1039
12. Aumailley, M., and Timpl, R. (1986) Attachment of cells to basement membrane collagen type IV. *J. Cell Biol.* **103**, 1569–1575
13. Hawkins, B. T., and Davis, T. P. (2005) The blood–brain barrier/neurovascular unit in health and disease. *Pharmacol. Rev.* **57**, 173–185
14. Hartmann, C., Zozulya, A., Wegener, J., and Galla, H. J. (2007) The impact of glia-derived extracellular matrices on the barrier function of cerebral endothelial cells: an in vitro study. *Exp. Cell Res.* **313**, 1318–1325
15. Tilling, T., Korte, D., Hoheisel, D., and Galla, H. J. (1998) Basement membrane proteins influence brain capillary endothelial barrier function in vitro. *J. Neurochem.* **71**, 1151–1157
16. Kröger, S., and Mann, S. (1996) Biochemical and functional characterization of basal lamina-bound agrin in the chick central nervous system. *Eur. J. Neurosci.* **8**, 500–509
17. Barber, A. J., and Lieth, E. (1997) Agrin accumulates in the brain microvascular basal lamina during development of the blood–brain barrier. *Dev. Dyn.* **208**, 62–74
18. Rascher, G., Fischmann, A., Kröger, S., Duffner, F., Grote, E. H., and Wolburg, H. (2002) Extracellular matrix and the blood–brain barrier in glioblastoma multiforme: spatial segregation of tenascin and agrin. *Acta Neuropathol.* **104**, 85–91
19. Berzin, T. M., Zipser, B. D., Rafii, M. S., Kuo-Leblanc, V., Yancopoulos, G. D., Glass, D. J., Fallon, J. R., and Stopa, E. G. (2000) Agrin and microvascular damage in Alzheimer's disease. *Neurobiol. Aging* **21**, 349–355
20. Arikawa-Hirasawa, E., Watanabe, H., Takami, H., Hassell, J. R., and Yamada, Y. (1999) Perlecan is essential for cartilage and cephalic development. *Nat. Genet.* **23**, 354–358
21. Costell, M., Gustafsson, E., Aszódi, A., Mörgelin, M., Bloch, W., Hunziker, E., Addicks, K., Timpl, R., and Fässler, R. (1999) Perlecan maintains the integrity of cartilage and some basement membranes. *J. Cell Biol.* **147**, 1109–1122
22. Roberts, J., Kahle, M. P., and Bix, G. J. (2012) Perlecan and the blood–brain barrier: beneficial proteolysis? *Front Pharmacol.* **3**, 155
23. Deguchi, Y., Okutsu, H., Okura, T., Yamada, S., Kimura, R., Yuge, T., Furukawa, A., Morimoto, K., Tachikawa, M., Ohtsuki, S., Hosoya, K., and Terasaki, T. (2002) Internalization of basic fibroblast growth factor at the mouse blood–brain barrier involves perlecan, a heparan sulfate proteoglycan. *J. Neurochem.* **83**, 381–389
24. Siddharthan, V., Kim, Y. V., Liu, S., and Kim, K. S. (2007) Human astrocytes/astrocyte-conditioned medium and shear stress enhance the barrier properties of human brain microvascular endothelial cells. *Brain Res.* **1147**, 39–50
25. Deli, M. A., Abrahám, C. S., Kataoka, Y., and Niwa, M. (2005) Permeability studies on in vitro blood-brain barrier models: physiology, pathology, and pharmacology. *Cell. Mol. Neurobiol.* **25**, 59–127
26. Weksler, B. B., Subileau, E. A., Perrière, N., Charneau, P., Holloway, K., Leveque, M., Tricoire-Leignel, H., Nicotra, A., Bourdoulous, S., Turowski, P., Male, D. K., Roux, F., Greenwood, J., Romero, I. A., and Couraud, P. O. (2005) Blood–brain barrier-specific properties of a human adult brain endothelial cell line. *FASEB J.* **19**, 1872–1874
27. An, Q., Fillmore, H. L., Vouri, M., and Pilkington, G. J. (2014) Brain tumor cell line authentication, an efficient alternative to capillary electrophoresis by using a microfluidics-based system. *Neuro Oncol.* **16**, 265–273
28. Maherally, Z., Smith, J. R., An, Q., and Pilkington, G. J. (2012) Receptors for hyaluronic acid and poliovirus: a combinatorial role in glioma invasion? *PLoS One* **7**, e30691
29. Weksler, B., Romero, I. A., and Couraud, P. O. (2013) The hCMEC/D3 cell line as a model of the human blood brain barrier. *Fluids Barriers CNS* **10**, 16
30. Chen, Y., and Liu, L. (2012) Modern methods for delivery of drugs across the blood–brain barrier. *Adv. Drug Deliv. Rev.* **64**, 640–665
31. Gaillard, P. J., Voorwinden, L. H., Nielsen, J. L., Ivanov, A., Atsumi, R., Engman, H., Ringbom, C., de Boer, A. G., and Breimer, D. D. (2001) Establishment and functional characterization of an in vitro model of

the blood–brain barrier, comprising a co-culture of brain capillary endothelial cells and astrocytes. *Eur. J. Pharm. Sci.* **12**, 215–222

32. Lee, D. S., Yu, K., Rho, J. Y., Lee, E., Han, J. S., Koo, D. B., Cho, Y. S., Kim, J., Lee, K. K., and Han, Y. M. (2006) Cyclopamine treatment of human embryonic stem cells followed by culture in human astrocyte medium promotes differentiation into nestin- and GFAP-expressing astrocytic lineage. *Life Sci.* **80**, 154–159

33. Yung, W. K., Luna, M., and Borit, A. (1985) Vimentin and glial fibrillary acidic protein in human brain tumors. *J. Neurooncol.* **3**, 35–38

34. Bergers, G., and Song, S. (2005) The role of pericytes in blood-vessel formation and maintenance. *Neuro Oncol.* **7**, 452–464

35. Nakagawa, S., Deli, M. A., Kawaguchi, H., Shimizudani, T., Shimono, T., Kittel, A., Tanaka, K., and Niwa, M. (2009) A new blood–brain barrier model using primary rat brain endothelial cells, pericytes and astrocytes. *Neurochem. Int.* **54**, 253–263

36. Engelhardt, B., and Sorokin, L. (2009) The blood–brain and the blood-cerebrospinal fluid barriers: function and dysfunction. *Semin. Immunopathol.* **31**, 497–511

37. Sixt, M., Engelhardt, B., Pausch, F., Hallmann, R., Wendler, O., and Sorokin, L. M. (2001) Endothelial cell laminin isoforms, laminins 8 and 10, play decisive roles in T cell recruitment across the blood–brain barrier in experimental autoimmune encephalomyelitis. *J. Cell Biol.* **153**, 933–946

38. Steiner, E., Enzmann, G. U., Lyck, R., Lin, S., Rüegg, M. A., Kröger, S., and Engelhardt, B. (2014) The heparan sulfate proteoglycan agrin contributes to barrier properties of mouse brain endothelial cells by stabilizing adherens junctions. *Cell Tissue Res.* **358**, 465–479

39. Wolburg, H., Noell, S., Wolburg-Buchholz, K., Mack, A., and Fallier-Becker, P. (2009) Agrin, aquaporin-4, and astrocyte polarity as an important feature of the blood-brain barrier. *Neuroscientist* **15**, 180–193

40. Gesemann, M., Brancaccio, A., Schumacher, B., and Ruegg, M. A. (1998) Agrin is a high-affinity binding protein of dystroglycan in non-muscle tissue. *J. Biol. Chem.* **273**, 600–605

41. Winkler, S., Stahl, R. C., Carey, D. J., and Bansal, R. (2002) Syndecan-3 and perlecan are differentially expressed by progenitors and mature oligodendrocytes and accumulate in the extracellular matrix. *J. Neurosci. Res.* **69**, 477–487

42. Fricker, G., Ott, M., and Mahringer, A. (2014). *The Blood–Brain Barrier (B–BB): An Introduction to Its Structure and Function. Topics in Medicinal Chemistry*, pp. 1–20, Springer-Verlag, Berlin

43. George, E. L., Georges-Labouesse, E. N., Patel-King, R. S., Rayburn, H., and Hynes, R. O. (1993) Defects in mesoderm, neural tube and vascular development in mouse embryos lacking fibronectin. *Development* **119**, 1079–1091

44. Pöschl, E., Schlötzer-Schrehardt, U., Brachvogel, B., Saito, K., Ninomiya, Y., and Mayer, U. (2004) Collagen IV is essential for basement membrane stability but dispensable for initiation of its assembly during early development. *Development* **131**, 1619–1628

45. Hatherell, K., Couraud, P. O., Romero, I. A., Weksler, B., and Pilkington, G. J. (2011) Development of a three-dimensional, all-human in vitro model of the blood–brain barrier using mono-, co-, and tri-cultivation transwell models. *J. Neurosci. Methods* **199**, 223–229

46. Nakagawa, S., Deli, M. A., Nakao, S., Honda, M., Hayashi, K., Nakaoke, R., Kataoka, Y., and Niwa, M. (2007) Pericytes from brain microvessels

47. Hayashi, K., Nakao, S., Nakaoke, R., Nakagawa, S., Kitagawa, N., and Niwa, M. (2004) Effects of hypoxia on endothelial/pericytic co-culture model of the blood-brain barrier. *Regul. Pept.* **123**, 77–83

48. Cohen-Kashi Malina, K., Cooper, I., and Teichberg, V. I. (2009) Closing the gap between the in-vivo and in-vitro blood–brain barrier tightness. *Brain Res.* **1284**, 12–21

49. Hayashi, Y., Nomura, M., Yamagishi, S., Harada, S., Yamashita, J., and Yamamoto, H. (1997) Induction of various blood–brain barrier properties in non-neural endothelial cells by close apposition to co-cultured astrocytes. *Glia* **19**, 13–26

50. Kacem, K., Lacombe, P., Seylaz, J., and Bonvento, G. (1998) Structural organization of the perivascular astrocyte endfeet and their relationship with the endothelial glucose transporter: a confocal microscopy study. *Glia* **23**, 1–10

51. Isobe, I., Watanabe, T., Yotsuyanagi, T., Hazemoto, N., Yamagata, K., Ueki, T., Nakanishi, K., Asai, K., and Kato, T. (1996) Astrocytic contributions to blood–brain barrier (BBB) formation by endothelial cells: a possible use of aortic endothelial cell for in vitro BBB model. *Neurochem. Int.* **28**, 523–533

52. Garcia, C. M., Darland, D. C., Massingham, L. J., and D'Amore, P. A. (2004) Endothelial cell-astrocyte interactions and TGFβ are required for induction of blood–neural barrier properties. *Brain Res. Dev. Brain Res.* **152**, 25–38

53. Yamamizu, K., Iwasaki, M., Takakubo, H., Sakamoto, T., Ikuno, T., Miyoshi, M., Kondo, T., Nakao, Y., Nakagawa, M., Inoue, H., and Yamashita, J. K. (2017) In vitro modeling of blood-brain barrier with human iPSC-derived endothelial cells, pericytes, neurons, and astrocytes via Notch signaling. *Stem Cell Reports* **8**, 634–647

54. Takata, F., Dohgu, S., Matsumoto, J., Takahashi, H., Machida, T., Wakigawa, T., Harada, E., Miyaji, H., Koga, M., Nishioku, T., Yamauchi, A., and Kataoka, Y. (2011) Brain pericytes among cells constituting the blood–brain barrier are highly sensitive to tumor necrosis factor-α, releasing matrix metalloproteinase-9 and migrating in vitro. *J. Neuroinflammation* **8**, 106

55. Winkler, E. A., Bell, R. D., and Zlokovic, B. V. (2011) Central nervous system pericytes in health and disease. *Nat. Neurosci.* **14**, 1398–1405

56. Daneman, R., Zhou, L., Kebede, A. A., and Barres, B. A. (2010) Pericytes are required for blood-brain barrier integrity during embryogenesis. *Nature* **468**, 562–566

57. Lai, C. H., and Kuo, K. H. (2005) The critical component to establish *in vitro* BBB model: pericyte. *Brain Res. Brain Res. Rev.* **50**, 258–265

58. Hori, S., Ohtsuki, S., Hosoya, K., Nakashima, E., and Terasaki, T. (2004) A pericyte-derived angiopoietin-1 multimeric complex induces occludin gene expression in brain capillary endothelial cells through Tie-2 activation in vitro. *J. Neurochem.* **89**, 503–513

59. Armulik, A., Genové, G., Mäe, M., Nisancioglu, M. H., Wallgard, E., Niaudet, C., He, L., Norlin, J., Lindblom, P., Strittmatter, K., Johansson, B. R., and Betsholtz, C. (2010) Pericytes regulate the blood–brain barrier. *Nature* **468**, 557–561